

Are the world's oceans optically different?

M. Szeto,¹ P. J. Werdell,² T. S. Moore,¹ and J. W. Campbell¹

Received 18 April 2011; revised 26 June 2011; accepted 11 July 2011; published 4 October 2011.

[1] Regional differences in the Sea-viewing Wide Field-of-view Sensor chlorophyll algorithm uncertainty were observed in a large global data set containing coincident in situ measurements of chlorophyll *a* concentration (*Chla*) and spectral radiometry. The uncertainty was found to be systematic when the data were sorted by ocean: Atlantic, Pacific, Southern, and Indian Oceans. Artifacts associated with different instrumentation and analytical methods had been previously ruled out. Given these oceanic biases in the chlorophyll algorithm, we hypothesized that the oceans may be optically different, and their optical differences may be intrinsically related to regional differences in phytoplankton community structure or biogeochemical processes. The oceanic biases, originally observed using radiometric measurements, were independently verified using total absorption measurements in a subset of the data. Moreover, they were explained through oceanic differences in the absorption of colored detrital matter (CDM) and phytoplankton. Both effects were considered together in explaining the ocean biases through a stepwise linear regression analysis. Significant oceanic differences in the amount of CDM and in phytoplankton cell sizes and pigmentation would give rise to optical differences, but we raise a concern for the spatial coverage of the data. We do not suggest the application of ocean-based algorithms but rather emphasize the importance of consolidating regional data sets before reaching this conclusion.

Citation: Szeto, M., P. J. Werdell, T. S. Moore, and J. W. Campbell (2011), Are the world's oceans optically different?, *J. Geophys. Res.*, 116, C00H04, doi:10.1029/2011JC007230.

1. Introduction

[2] There exists great interest in utilizing ocean color radiometry to discern the ecological provinces of the ocean [International Ocean Colour Coordinating Group, 2009]. Such a capability lends considerable potential for understanding the structure of global marine ecosystems and for mapping the dynamic biogeography of the sea. Ultimately, the success of this endeavor rests on whether regional differences in ocean color are intrinsically related to regional differences in marine ecological and biogeochemical processes.

[3] Regional differences in ocean color can be recognized through assessments of algorithm biases using the global sample of observations in NASA Bio-optical Marine Algorithm Data Set (NOMAD) [Werdell and Bailey, 2005]. This data set contains coincident in situ measurements of the phytoplankton biomass (approximated as the concentration of chlorophyll *a* pigments, hereafter denoted as *Chla*), and spectral radiometry for the intensity of light upwelled from below the ocean surface (i.e., the ocean color).

[4] Algorithms used to derive *Chla* from satellite radiometry have been parameterized using NOMAD. When the data set is analyzed as a whole, the OC4 algorithm used for processing Sea-viewing Wide Field-of-view Sensor (SeaWiFS) data has an uncertainty greater than 50% [Moore *et al.*, 2009]. However, errors are not random but rather exhibit systematic trends when the data are sorted by the Atlantic, Pacific, Southern, and Indian Oceans (Figure 1). The algorithm underestimates *Chla* for stations from the Pacific, Indian, and Southern Oceans by 15, 17, and 50%, respectively, and overestimates *Chla* for the Atlantic Ocean stations by 14%. These systematic deviations by ocean are denoted hereafter as the oceanic biases.

[5] The data in NOMAD were contributed by numerous investigators who used a variety of methods and instruments. To investigate whether the oceanic biases might be artifacts of methodological differences, an analysis of variance (ANOVA) was performed in an earlier study (M. Szeto, Reducing the uncertainty in the MODIS and SeaWiFS chlorophyll algorithms, Research and Discover University of New Hampshire-NASA Program Project, 2006, available at http://www.eos.unh.edu/ResearchAndDiscover/interns_06_07.shtml#mimi) to test for the effects of three factors: the brand of the radiometer used, whether the radiometer was the above or below water type, and whether the *Chla* measurements were made either fluorometrically or by high-pressure liquid chromatography (HPLC). Based on the ANOVA results, effects from these factors were found to be insignificant (M. Szeto, research project, 2006). Moreover, we performed the ANOVA to test

¹Ocean Process Analysis Laboratory, Institute for the Study of Earth, Oceans, and Space, University of New Hampshire, Durham, New Hampshire, USA.

²Ocean Biology Processing Group, NASA Goddard Space Flight Center, Greenbelt, Maryland, USA.

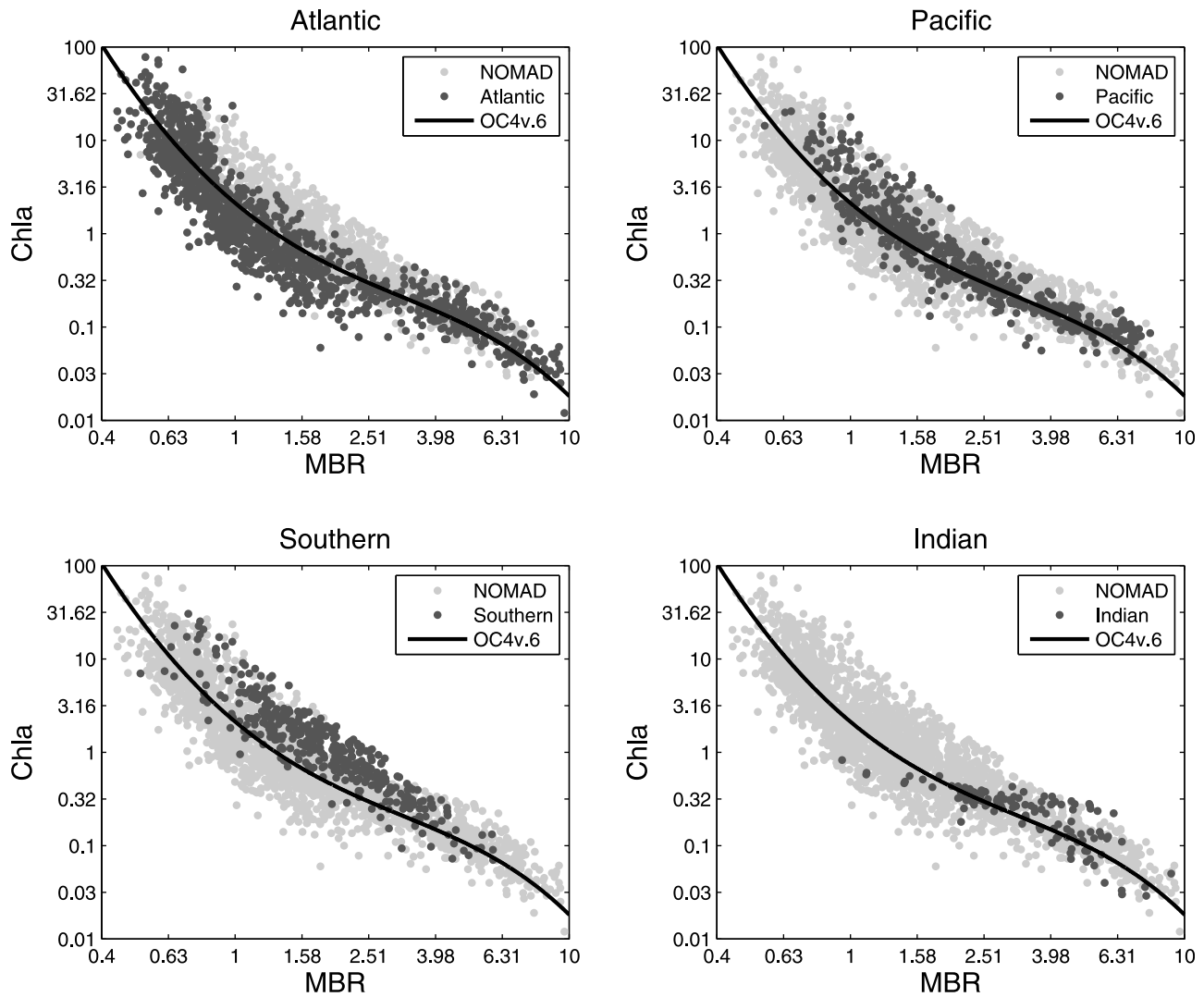


Figure 1. NOMAD with OC4v.6: the oceanic biases. *Chla* is plotted against the maximum band ratio ($MBR = \max[R_{rs}(443), R_{rs}(490), R_{rs}(510)]$). The oceanic biases are illustrated. The light grey points represent all the data ($n = 2365$), and the dark grey points represent the data from the specified ocean. The solid curve represents the OC4v.6 algorithm. Note that the axes have logarithmic scales.

for the effect of the project investigator, which represents a consolidation of all methodological artifacts, and found this to be insignificant as well (M. Szeto, research project, 2006). The oceanic biases were present in the data from the same investigator contributing to more than one ocean, and from different investigators in the same ocean.

[6] From the recognition of these regional differences in bio-optics arises the question: Are the world's oceans, in fact, optically different? In other words, are these oceanic biases related to regional differences in the inherent optical properties (i.e., absorption and scattering by the constituents in the ocean)? And if so, why?

[7] Based on the community's literature on bio-optics theory and empirical region-based differences in bio-optics [Darecki and Stramski, 2004; D'Ortenzio et al., 2002; Garcia et al., 2005; Gohin et al., 2002; Morel and Maritorena, 2001; Morel et al., 2007; Siegel et al., 2002; Kahru and Mitchell,

1999; Mitchell and Holm-Hansen, 1991; Mitchell and Kiefer, 1988a; Dmitriev et al., 2009; Lutz et al., 2006; Pan et al., 2008; Ahn et al., 2008; Fenton et al., 1994; Werdell et al., 2009], it was hypothesized that the systematic deviation by ocean could be explained by systematic variation in the amount of nonalgal dissolved and particulate matter (denoted hereafter as colored detrital matter (CDM)) or variation in the phytoplankton community structure. The latter explanation is supported by several works which found that the magnitude of pigment-specific particulate absorption in various locales varies tenfold as a result of variations in pigment packaging, species composition, and the abundance of detrital matter relative to phytoplankton biomass [Mitchell and Holm-Hansen, 1991; Maske and Haardt, 1987; Mitchell and Kiefer, 1988a, 1988b; Bricaud et al., 1988; Morrow et al., 1989; Bricaud and Stramski, 1990].

[8] The work reported here represents an attempt to investigate the topic of regional differences in optics and

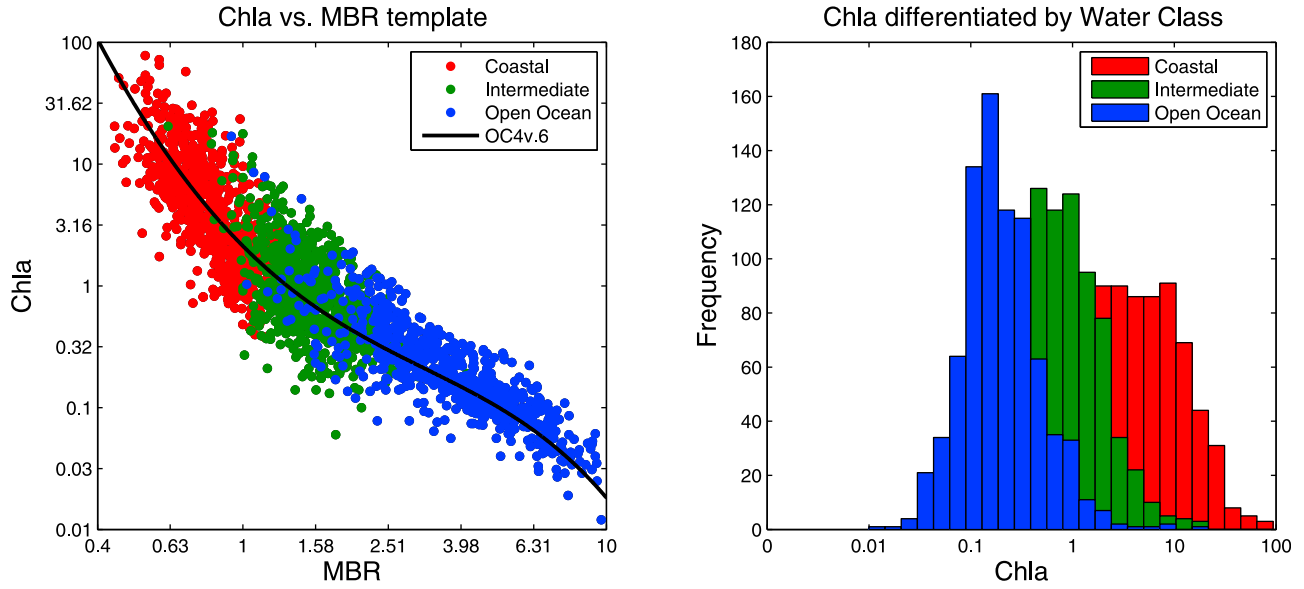


Figure 2. The water classes. The three water classes are differentiated (left) in the plot of *Chla* versus MBR and (right) in a histogram. They are defined in terms of the maximum band ratio used, color coded here with blue indicating open ocean, green indicating intermediate, and red indicating coastal. These classes roughly correspond to oligotrophic, mesotrophic, and eutrophic regions, respectively. Plots of *Chla* versus MBR such as Figure 2 (left) will be used as a template to show trends in the various optical properties related to the ocean biases. The points are NOMAD data ($n = 2365$), and the solid curve is the OC4v.6 algorithm. Points above the curve are underestimated by the algorithm, whereas points below the curve are overestimated. Note that the *Chla* and MBR axes have logarithmic scales.

biogeochemistry using in situ data on a comprehensive scale. Presented next is the mathematical framework which includes bio-optics theory and definitions for algorithm uncertainty, followed by the methods, results, discussion and conclusion.

2. Mathematical Framework

2.1. Bio-optics Theory

[9] The remote sensing reflectance, defined as the ratio of upwelling radiance to downwelling irradiance, is related to inherent optical properties (IOPs) by the expression [Morel, 1980; Gordon *et al.*, 1988]

$$r_{rs}(\lambda) \sim \frac{b_b(\lambda)}{a(\lambda) + b_b(\lambda)}. \quad (1)$$

Here, r_{rs} represents the subsurface remote sensing reflectance calculated from radiometric measurements made just below the surface. The terms a and b_b represent the total absorption and backscattering coefficients, respectively, and they are derivatives of absorbance and backscatterance with respect to a given path length [Kirk, 1994]. Note that all terms are spectrally dependent as indicated by the λ notation. Assuming that sea-air transmittance is nonspectral, the same statement can be made about above water reflectance, R_{rs} , and this is often the basis for semianalytic algorithms [Lee *et al.*, 2002; Maritorena *et al.*, 2002].

[10] While this theory is arguably well understood [Gordon *et al.*, 1988; Zaneveld, 1995], its application to ocean color algorithms has yet to show significant improvement in esti-

imating *Chla* compared to empirical methods that simply rely on the statistical relationship found between R_{rs} and *Chla*. Used for the analysis featured here, OC4v.6, an algorithm designed for SeaWiFS, is expressed mathematically by a fourth-order polynomial function [O'Reilly *et al.*, 2002]

$$\log_{10}(\text{Chla}) = 0.3272 - 2.9940X + 2.7218X^2 - 1.2259X^3 - 0.5683X^4, \quad (2)$$

where X is the base 10 logarithm of a maximum band ratio (MBR) defined by the following:

$$X = \log_{10} \left(\frac{\max[R_{rs}(443), R_{rs}(490), R_{rs}(510)]}{R_{rs}(555)} \right). \quad (3)$$

[11] In this work, three water classes, open ocean, intermediate, and coastal, were defined by the maximum R_{rs} used to calculate X : open ocean for the $R_{rs}(443)$, intermediate for $R_{rs}(490)$, and coastal for $R_{rs}(510)$. Figure 2 illustrates the water classes with respect to the relationship between *Chla* and MBR. The histograms suggest that these water classes roughly correspond to oligotrophic, mesotrophic, and eutrophic regions, respectively. Note that the biases seen in Figure 1 are primarily located in intermediate and coastal areas, which are overrepresented by the NOMAD data [Moore *et al.*, 2009].

[12] We provide in the Appendix coefficients for ocean-specific OC4 algorithms. These algorithms are presented for the purpose of demonstrating the oceanic biases relative to the global algorithm. They may be applied to SeaWiFS data in regions represented by the NOMAD stations, but caution

Table 1. Statistics of Δ and \hat{C}_i/C_i for NOMAD, $n = 2365$, Sorted by Ocean and Water Class^a

Water Class	Ocean	n	Δ			\hat{C}_i/C_i		
			Mean	SD	RMSE	Lower Limit	Median	Upper Limit
All	Atlantic	1249	0.082	0.264	0.276	0.657	1.207	2.216
	Pacific	595	-0.094	0.211	0.231	0.495	0.805	1.309
	Indian	121	-0.049	0.187	0.193	0.581	0.894	1.376
	Southern	400	-0.302	0.212	0.369	0.306	0.499	0.812
	Global	2365	-0.034	0.278	0.280	0.487	0.924	1.755
Coastal	Atlantic	626	0.086	0.295	0.308	0.617	1.218	2.405
	Pacific	94	-0.103	0.240	0.261	0.454	0.789	1.371
	Indian	2	0.448	0.057	0.452	2.461	2.805	3.198
	Southern	64	-0.303	0.294	0.422	0.253	0.498	0.979
	Global	786	0.032	0.312	0.314	0.526	1.078	2.210
Intermediate	Atlantic	317	0.160	0.236	0.285	0.838	1.444	2.487
	Pacific	242	-0.144	0.245	0.284	0.408	0.718	1.261
	Indian	33	0.022	0.113	0.116	0.811	1.053	1.367
	Southern	178	-0.341	0.179	0.385	0.302	0.456	0.688
	Global	770	-0.057	0.300	0.306	0.439	0.876	1.750
Open Ocean	Atlantic	306	-0.007	0.185	0.185	0.642	0.983	1.506
	Pacific	259	-0.045	0.145	0.152	0.647	0.902	1.260
	Indian	86	-0.087	0.188	0.207	0.531	0.818	1.261
	Southern	158	-0.258	0.199	0.326	0.349	0.552	0.872
	Global	809	-0.077	0.199	0.213	0.530	0.838	1.325

^aSD is standard deviation.

is advised at locations outside those regions. A map of the stations' locations is given by *Werdell and Bailey* [2005].

2.2. Definition of the Algorithm Uncertainty

[13] Algorithm uncertainty was characterized using the difference between log-transformed estimates of *Chla*, which is expressed as Δ

$$\Delta_i = \log_{10}(\hat{C}_i) - \log_{10}(C_i), \quad (4)$$

where i refers to a particular observation, \hat{C}_i the algorithm estimate, and C_i the corresponding in situ measurement. Note that Δ is equivalent to $\log_{10}(\hat{C}_i/C_i)$. Without loss of generality, \hat{C}_i/C_i will serve as the nonlogarithm representation of algorithm uncertainty.

[14] In assessing the algorithm uncertainty for a given sample of *Chla*, the mean Δ represents the algorithm bias and the root-mean-square Δ (RMSE) represents the combined uncertainty from both the bias and the standard deviation. The algorithm exhibits an overestimation when $\Delta > 0$ and an underestimation when $\Delta < 0$.

[15] The statistic Δ is approximately normally distributed with mean m and standard deviation s , and thus, the ratio, \hat{C}_i/C_i , is log normally distributed [Campbell, 1995]. To interpret statistics for Δ in terms of relative error as is commonly desired, the following calculations were made:

$$\text{lower limit} = 10^{m-s} \quad (5)$$

$$\text{median } \hat{C}_i/C_i = 10^m \quad (6)$$

$$\text{upper limit} = 10^{m+s} \quad (7)$$

[16] The upper and lower limits represent \pm one standard deviation about the mean of Δ , and assuming a normal distribution, they bound the inner 68% of the distribution of \hat{C}_i/C_i with equal portions above and below the median.

Statistics for the NOMAD ($n = 2365$) data set are shown in Table 1.

3. Methods

[17] The investigation involved analyses of inherent optical property (IOP) data available in NOMAD to verify the existence of the oceanic biases and to understand their source. Since IOPs are measured independently from the radiometric measurements, biases in the IOPs would verify the existence of the oceanic biases.

[18] To examine whether oceanic biases are present in the IOP data, the following IOP-based approximation was used

$$\frac{R_{rs}(\lambda)}{R_{rs}(555)} \sim \frac{a_{tot}(555)b_b(\lambda)}{a_{tot}(\lambda)b_b(555)} \sim \frac{a_{tot}(555)}{a_{tot}(\lambda)}. \quad (8)$$

[19] Ultimately, the a_{tot} ratio was used to analyze for oceanic biases in absorption. There was insufficient b_b data to use the ratio involving both IOP measurements. However, we used several backscattering models to analyze the effect of variability in the backscattering ratio.

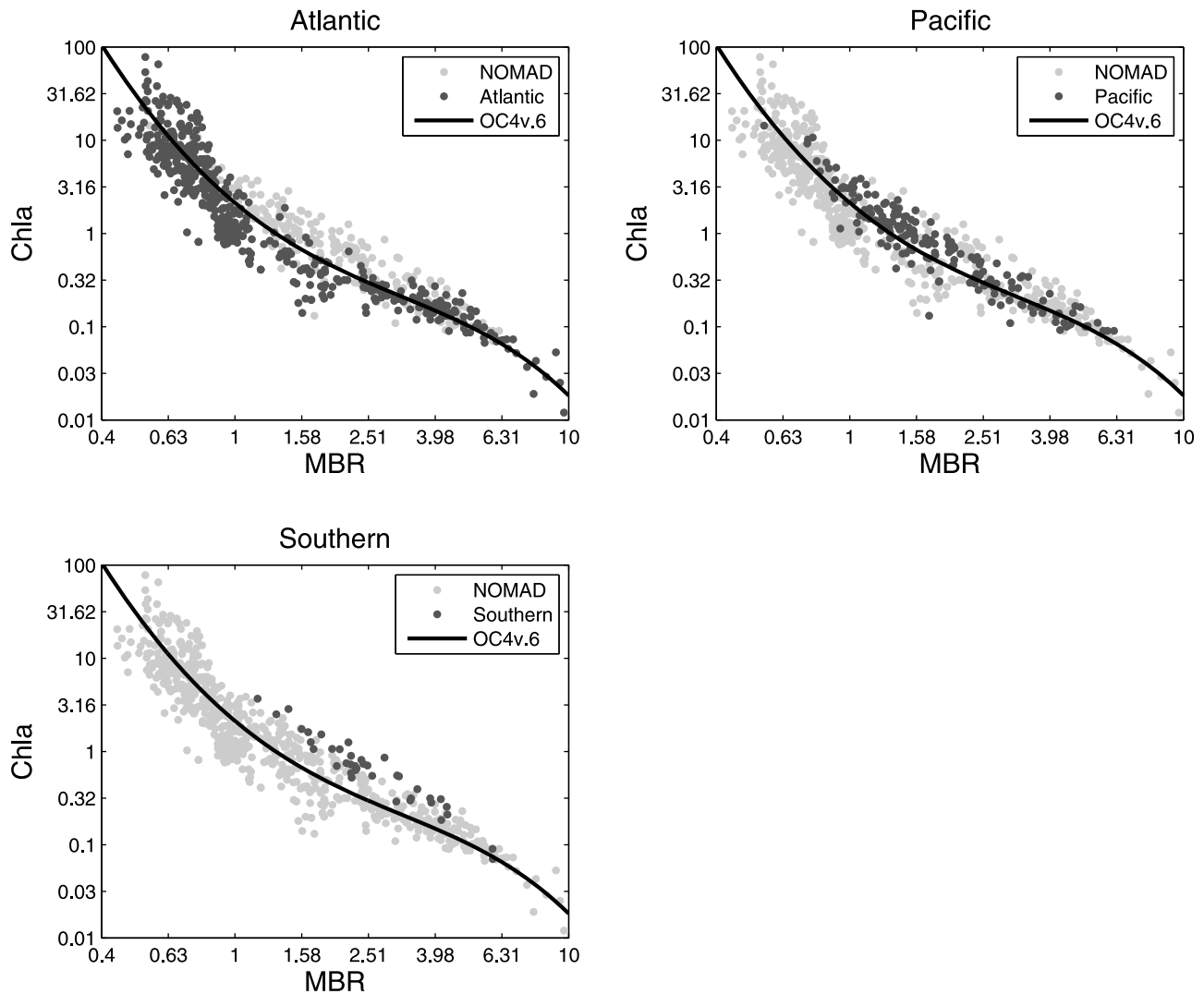
3.1. Oceanic Biases in Absorption

[20] The NOMAD data set contains a subset of stations ($n = 696$) with coincident measurements of total absorption (a_{tot}), and its components, colored dissolved organic matter (a_{cdom}), nonalgal particulates (a_{nap}), and phytoplankton (a_{ph}), at the 20 wavelengths used for various satellite sensors [Werdell, 2005]. These measurements were integrated over the first optical depth [Werdell, 2005]. Though much smaller in size, this subset still exhibits the oceanic biases, particularly for the Atlantic and Pacific Oceans in the intermediate water class (Table 2 and Figure 3). Note that there was only one Indian Ocean station with absorption measurements and it was not included in the analysis.

[21] The a_{tot} ratio approximation serves as a way to represent MBR in terms of the absorption data available in

Table 2. Statistics of Δ and \hat{C}_i/C_i for the NOMAD Subset, $n = 696$, Containing IOP Data^a

Water Class	Ocean	n	Δ			\hat{C}_i/C_i		
			Mean	SD	RMSE	Lower Limit	Median	Upper Limit
All	Atlantic	478	0.087	0.247	0.262	0.692	1.222	2.158
	Pacific	179	-0.079	0.159	0.178	0.578	0.834	1.203
	Southern	39	-0.315	0.126	0.339	0.363	0.485	0.647
	Global	696	0.022	0.247	0.248	0.596	1.052	1.858
Coastal	Atlantic	296	0.104	0.280	0.298	0.666	1.269	2.417
	Pacific	38	-0.071	0.145	0.161	0.608	0.849	1.185
	Southern	0	—	—	—	—	—	—
	Global	334	0.084	0.273	0.286	0.646	1.212	2.276
Intermediate	Atlantic	81	0.151	0.198	0.249	0.897	1.416	2.233
	Pacific	75	-0.100	0.181	0.207	0.523	0.794	1.205
	Southern	18	-0.340	0.099	0.354	0.364	0.457	0.574
	Global	174	-0.008	0.245	0.245	0.558	0.981	1.727
Open Ocean	Atlantic	101	-0.012	0.120	0.120	0.739	0.973	1.283
	Pacific	66	-0.059	0.137	0.15	0.636	0.872	1.197
	Southern	21	-0.292	0.143	0.326	0.367	0.510	0.71
	Global	188	-0.060	0.154	0.165	0.611	0.871	1.243

^aSD is standard deviation.**Figure 3.** NOMAD subset ($n = 696$) with OC4v.6, differentiated by ocean. The light grey points represent all the data in the subset, and the dark grey points represent the data from the specified ocean. The solid curve represents the OC4v.6 algorithm. Note that the axes have logarithmic scales.

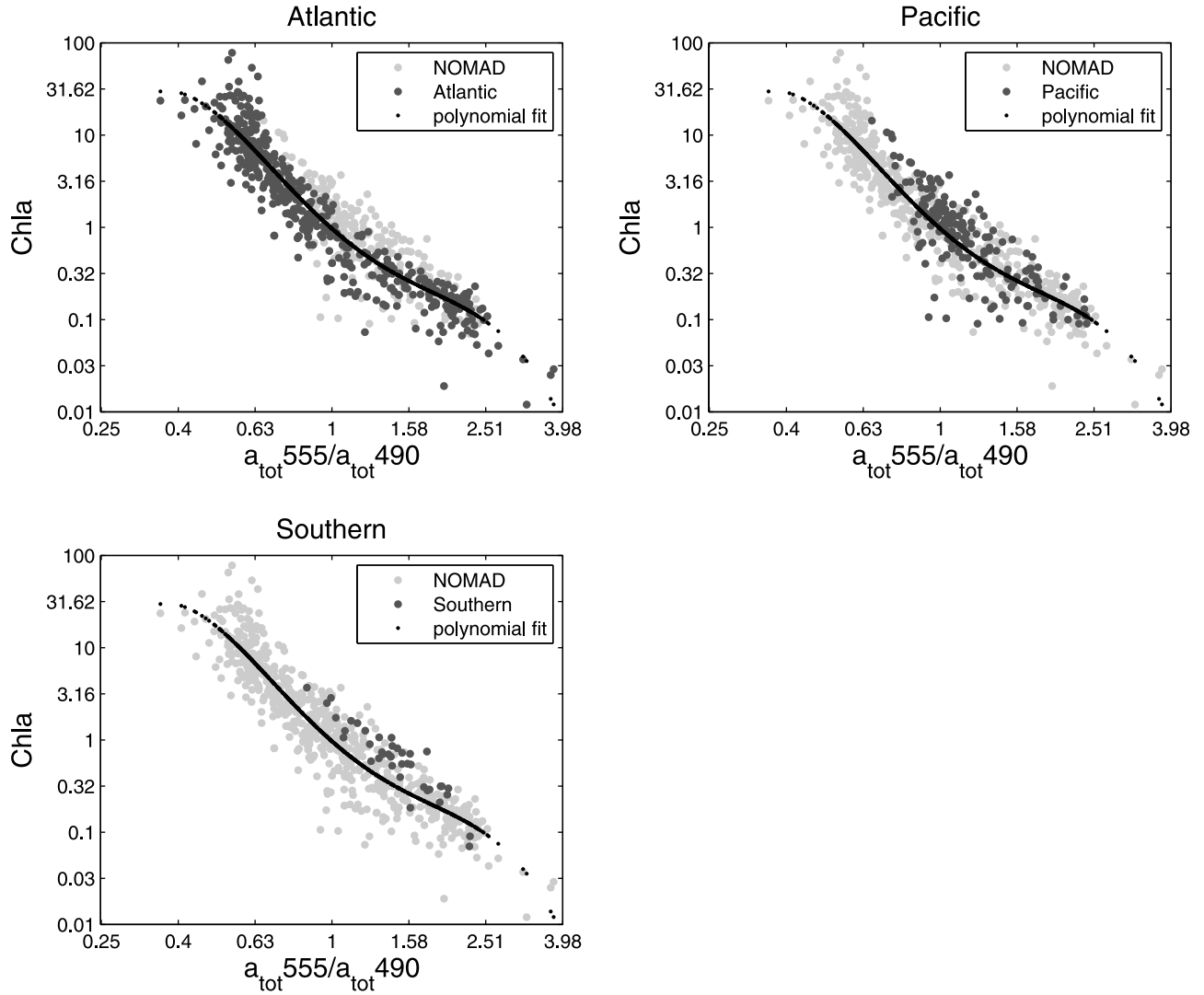


Figure 4. NOMAD subset ($n = 696$) with the fit for $Chla$ versus $\frac{a_{tot}(555)}{a_{tot}(490)}$, differentiated by ocean. The light grey points represent all the data in the subset, and the dark grey points represent the data from the specified ocean. The solid curve represents the fourth-order polynomial fit to the relationship between $Chla$ and $\frac{a_{tot}(555)}{a_{tot}(490)}$. Note that the axes have logarithmic scales.

NOMAD. By using the same wavelength used to calculate the maximum band ratio: 443, 490, or 510, the approximation best represents the MBR. However, ratios involving a fixed wavelength were also considered. In each case, a fourth-order polynomial was fitted to the relationship between $Chla$ and the a_{tot} ratio, and the data were sorted by ocean.

3.2. Effect of Variation in Backscattering

[22] The backscattering measurements in NOMAD ($n = 80$) were not sufficient to incorporate into the approximation. However, to consider the effects of the backscattering ratio in equation (8), we modeled b_b in two ways: (1) $b_{bp}(490)$ and $b_{bp}(555)$ as functions of $Chla$ [Morel and Maritorena, 2001] and (2) by modeling $b_{bp}(555)$ as a function of $Chla$ [Morel and Maritorena, 2001] and $b_{bp}(\lambda) = b_{bp}(555)\lambda^{-\eta}$. The exponent η was modeled as a function of the subsurface reflectance ratio, $\frac{r_{rs}(443)}{r_{rs}(555)}$ [Lee et al., 2010]. The backscattering

coefficient of pure water, b_{bw} , modeled according to Morel [1974], was added to b_{bp} to obtain b_b .

3.3. Understanding the Source of the Oceanic Biases

[23] Variations in CDM and the phytoplankton community structure were represented using the parameters $a_{cdm}443/Chla$ and $a_{ph}443/Chla$, where a_{cdm} is the sum of a_{cdm} and a_{nap} . Both $a_{cdm}443/Chla$ and $a_{nap}443/Chla$ were also considered independently. The wavelength 443 nm was chosen because a change in abundance of either CDM or phytoplankton is better represented at this wavelength compared to others. The purpose of the normalization by in situ $Chla$ in the parameters $a_{cdm}443/Chla$ and $a_{ph}443/Chla$ is to link these ratios to \hat{C}_i/C_i , the algorithm uncertainty expressed as the algorithm-derived $Chla$ normalized by in situ $Chla$. Patterns in the algorithm uncertainty related to these two parameters

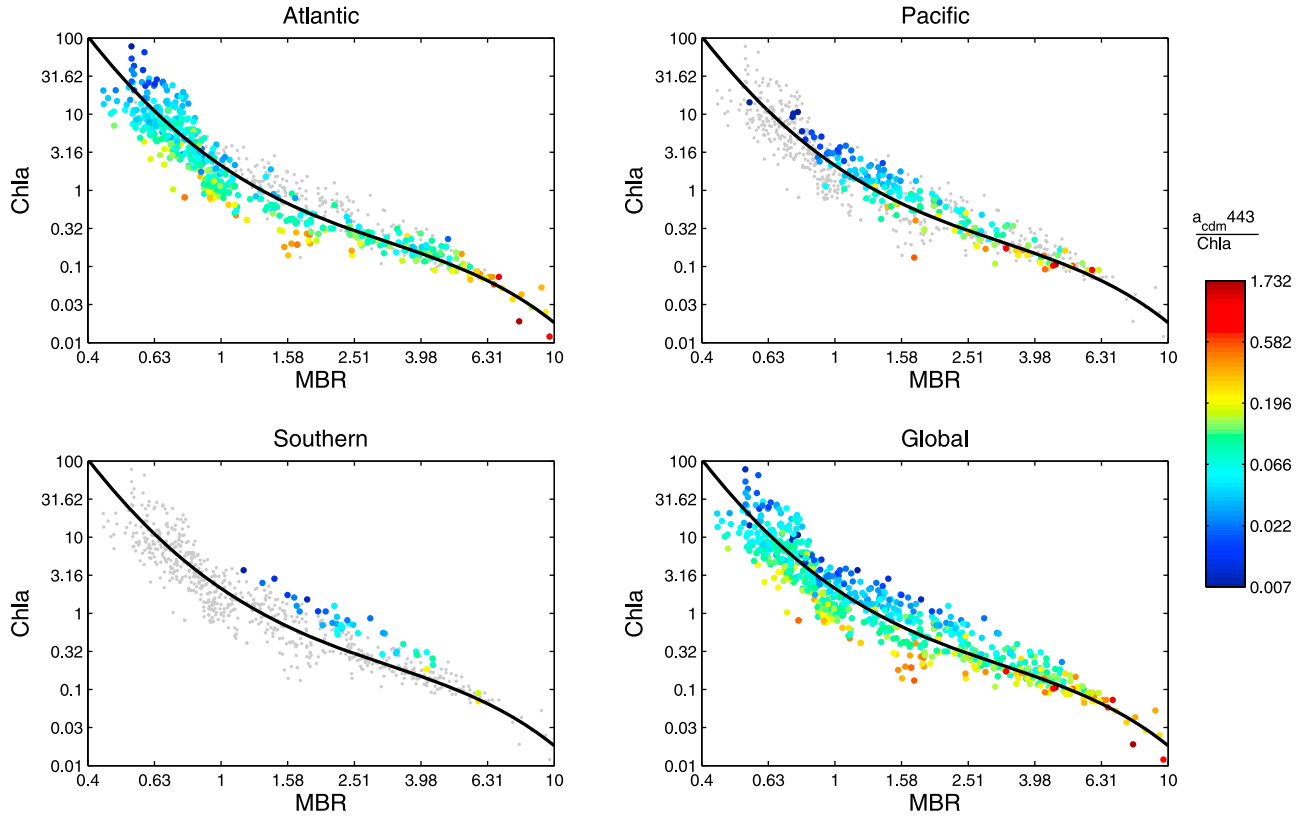


Figure 5. The effects of CDM on the oceanic biases: $a_{cdm}443/Chla$. Systematic variation in $a_{cdm}443/Chla$, as color coded, corresponds to variation above and below the algorithm curve, i.e., variation in Δ for NOMAD ($n = 696$). Note that the axes and color scales are logarithmic. The solid curve represents the OC4v.6 algorithm.

were analyzed both visually and quantitatively using statistical measures.

[24] To evaluate the combined effects, a stepwise ordinary least squares linear regression was used to examine the relative importance of the two effects. The regression is defined as the following:

$$\Delta = b_1 + b_2 \log_{10} \left(\frac{a_{ph}443}{Chla} \right) + b_3 \log_{10} \left(\frac{a_{cdm}443}{Chla} \right), \quad (9)$$

where b_1 , b_2 , and b_3 are resulting coefficients from each analysis. Specifically, we used the MATLAB routine “stepwise fit,” (2007, MathWorks, Natick, Massachusetts) with default settings.

[25] In the stepwise regression, the parameter with the higher correlation with Δ is used to predict Δ in the first step. This parameter explains more of the variance of Δ than the other. Then, the second parameter is added if it significantly reduces the residuals. The significance is based on a comparison of the variance (F test) with or without the potential parameter ($P < 0.05$).

[26] A common misconception is that the coefficients from the regression analyses indicate the relative importance of the effects. Rather, the coefficients are affected by the relative magnitudes of $a_{cdm}443/Chla$ and $a_{ph}443/Chla$, whereas the sequence of parameters used in the model indicates their relative importance. The parameter used to fit the initial

model of every stepwise regression is the parameter with the greater influence on algorithm uncertainty.

4. Results

4.1. Oceanic Biases in Absorption

[27] Oceanic biases were present when using the absorption-based approximation to MBR, as illustrated for $\lambda = 490$ nm in Figure 4. These biases were comparable to those about the OC4 algorithm when using all wavelength combinations. The replacement of MBR with the total absorption approximation served as an independent method to verify the existence of the oceanic biases, and indicates that these biases are related to true (inherent) optical differences among the oceans.

4.2. Effect of Variation in Backscattering

[28] Using both the absorption and modeled backscattering coefficients in the approximation of MBR resulted in minor changes to results shown in Figure 4. Polynomials fitted to the IOP ratio, for various b_b models and wavelengths, improved the correlation by 4 to 12%. The ocean biases remained unchanged.

4.3. Understanding the Source of the Oceanic Biases

4.3.1. Effects of Colored Detrital Matter

[29] The effect of CDM on the algorithm uncertainty is demonstrated in Figure 5. As shown in the Global plot of

Table 3. The Effects of CDM and Phytoplankton Community Structure on the Oceanic Biases: $a_{cdm}443/Chl$ and $a_{ph}443/Chl^a$

Water Class	Ocean	n	$\frac{a_{cdm}443}{Chla}$			$\frac{a_{ph}443}{Chla}$		
			Lower Limit	Median	Upper Limit	Lower Limit	Median	Upper Limit
All	Atlantic	478	0.049	0.096	0.190	0.032	0.055	0.092
	Pacific	179	0.025	0.067	0.179	0.030	0.049	0.080
	Southern	39	0.018	0.041	0.089	0.032	0.044	0.061
	Global	696	0.037	0.084	0.187	0.032	0.053	0.087
Coastal	Atlantic	296	0.043	0.080	0.146	0.027	0.042	0.065
	Pacific	38	0.014	0.026	0.050	0.023	0.037	0.059
	Southern	0	—	—	—	—	—	—
	Global	334	0.035	0.070	0.142	0.026	0.041	0.064
Intermediate	Atlantic	81	0.062	0.117	0.220	0.053	0.075	0.107
	Pacific	75	0.030	0.064	0.137	0.026	0.042	0.066
	Southern	18	0.013	0.025	0.047	0.029	0.039	0.053
	Global	174	0.034	0.077	0.177	0.033	0.055	0.090
Open Ocean	Atlantic	101	0.069	0.141	0.291	0.07	0.092	0.121
	Pacific	66	0.050	0.123	0.305	0.052	0.070	0.094
	Southern	21	0.032	0.062	0.120	0.036	0.049	0.066
	Global	188	0.054	0.123	0.279	0.055	0.078	0.111

^aThe median and standard deviations above and below the median are presented for $a_{cdm}443/Chla$ and $a_{ph}443/Chla$. See equations (5)–(7).

this figure, the algorithm overestimates $Chla$ at stations with relatively high values of $a_{cdm}443/Chla$, and underestimates $Chla$ where $a_{cdm}443/Chla$ is relatively low. The effect is clear for the coastal and intermediate stations and less so for the open ocean stations. The other plots in Figure 5 show that this pattern corresponds with the biases in the respective oceans.

[30] Quantitative analysis confirms the results; Table 3 shows the results sorted by water class and ocean. Of the three water classes, the intermediate class had the strongest biases. In this class, the Southern Ocean stations, which are underestimated by the algorithm, have a relatively low median $a_{cdm}443/Chla$ of 0.025, while the Atlantic Ocean stations, which are overestimated by the algorithm, have a

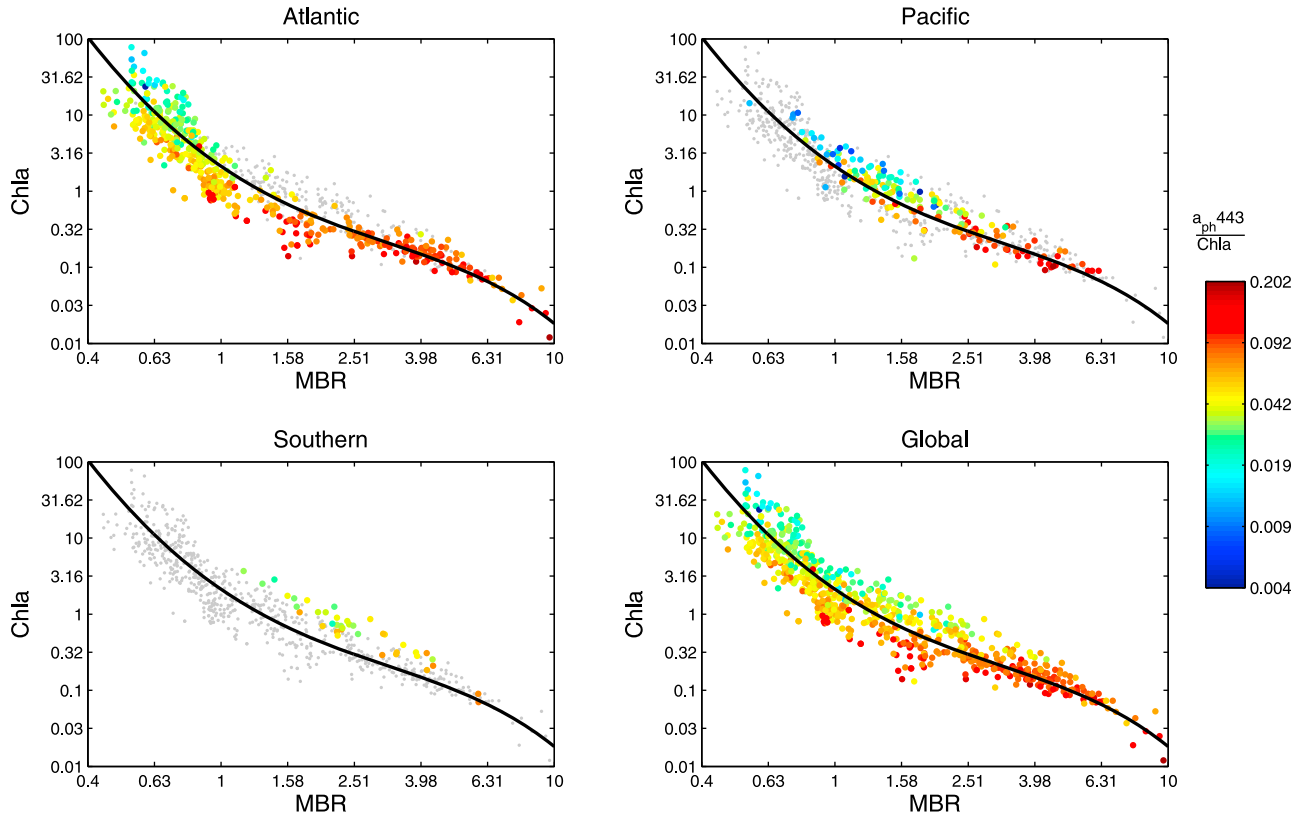


Figure 6. The effects of pigment packaging on the oceanic biases: $a_{ph}443/Chla$. Systematic variation in $a_{ph}443/Chla$, as color coded, corresponds to variation above and below the algorithm curve, i.e., variation in Δ for NOMAD ($n = 696$). Note that the axes and color scales are logarithmic. The solid curve represents the OC4v.6 algorithm.

Table 4. Coefficients of Determination (r^2) Among In Situ Absorption and *Chla* Measurements^a

Water Class	Ocean	<i>n</i>	$\log_{10}Chla$,	$\log_{10}Chla$,	$\log_{10}a_{cdm443}$,
			$\log_{10}a_{cdm443}$	$\log_{10}a_{ph443}$	$\log_{10}a_{ph443}$
All	Atlantic	478	0.86	0.95	0.86
	Pacific	179	0.24	0.84	0.19
	Southern	39	0.16	0.88	0.07
	Global	696	0.75	0.93	0.78
Coastal	Atlantic	296	0.66	0.83	0.66
	Pacific	38	0.15	0.56	0.02
	Southern	0	—	—	—
	Global	334	0.53	0.82	0.59
Intermediate	Atlantic	81	0.22	0.70	0.30
	Pacific	75	0.03	0.54	0.01
	Southern	18	0.01	0.73	0.00
	Global	174	0.05	0.57	0.07
Open Ocean	Atlantic	101	0.10	0.82	0.08
	Pacific	66	0.04	0.90	0.06
	Southern	21	0.20	0.87	0.05
	Global	188	0.13	0.83	0.12

^aThe r^2 values for correlations among the logarithms of *Chla*, a_{cdm443} , and a_{ph443} are presented here. For each column heading, the correlated properties are separated by a comma.

relatively high median $a_{cdm443}/Chla$ of 0.117. The Pacific Ocean stations, which are slightly underestimated by the algorithm, have a median $a_{cdm443}/Chla$ (0.064) falling between the other two. The other ocean classes show similar regional variation.

[31] The values for a_{nap} and a_{cdm} are often combined because they have similar spectral shapes. When $a_{nap443}/Chla$ and $a_{cdm443}/Chla$ were considered separately, the results for $a_{cdm443}/Chla$ were similar to those for $a_{cdm443}/Chla$. The results for $a_{nap443}/Chla$ were similar in the intermediate and open ocean classes, where a_{nap443} was less than 20% of a_{cdm443} . In the coastal class waters, where a_{nap443} was as much as 50% of a_{cdm443} , there was no systematic variation with Δ .

4.3.2. Effects of Phytoplankton Community Structure

[32] Figure 6 presents the qualitative analysis for $a_{ph443}/Chla$. The Global plot of this figure clearly reveals that the pigment effect (i.e., pigment packaging and the presence of accessory pigments, both indicative of variations in community structure) systematically varies with the shift in algorithm uncertainty for all water classes. The parameter $a_{ph443}/Chla$ is relatively high at stations where *Chla* is overestimated by the algorithm and low where *Chla* is underestimated. Similar to the results for $a_{cdm443}/Chla$ the other plots in Figure 6 show that this pattern corresponds with the biases in the respective oceans.

[33] Quantitative results for the water classes and oceans are shown in Table 3. Results for the intermediate class, which had the strongest biases, are described here. The Southern Ocean stations, which are underestimated by the algorithm, have a relatively low median $a_{ph443}/Chla$ of 0.039, while the Atlantic Ocean stations, which are overestimated by the algorithm, have a relatively high median $a_{ph443}/Chla$ of 0.075, about twice the

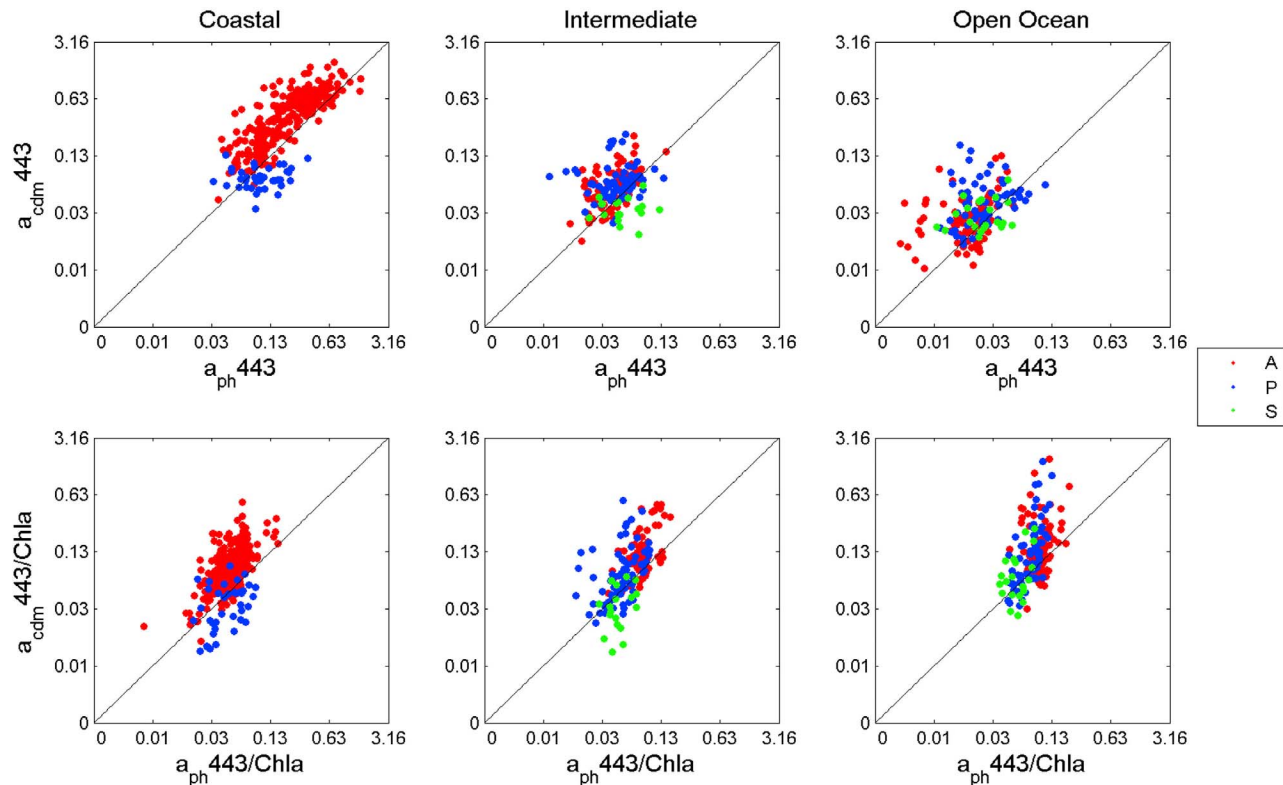


Figure 7. Relationship between a_{cdm443} and a_{ph443} with and without normalization by *Chla*. The relationships (top) between a_{ph443} and a_{cdm443} and (bottom) between the parameters, $a_{ph443}/Chla$ and $a_{cdm443}/Chla$, are presented. Data are sorted by water class, and color coded for the oceans: red, Atlantic (A); blue, Pacific (P); green, Southern (S). Note that the axes are logarithmic.

Table 5. The Relative Importance of CDM and Community Structure: Regression Statistics^a

Water Class	Ocean	b_1	$b_2(\pm SD)$	$b_3(\pm SD)$	n	r^2
All	Global	0.535	0.135(± 0.045)	0.315(± 0.028)	696	0.28
Coastal	Atlantic	1.324	0.572(± 0.081)	0.393(± 0.059)	296	0.47
	Pacific	0.407	—	0.301(± 0.069)	38	0.33
	Southern	—	—	—	—	—
Intermediate	Global	1.232	0.531(± 0.069)	0.357(± 0.043)	334	0.47
	Atlantic	0.668	—	0.555(± 0.052)	81	0.58
	Pacific	0.650	0.261(± 0.078)	0.327(± 0.048)	75	0.56
	Southern	0.421	0.229(± 0.089)	0.273(± 0.042)	18	0.80
Open Ocean	Global	0.910	0.343(± 0.056)	0.436(± 0.033)	174	0.74
	Atlantic	0.471	0.409(± 0.092)	0.071(± 0.035)	101	0.21
	Pacific	0.113	—	0.190(± 0.037)	66	0.29
	Southern	0.689	0.473(± 0.141)	0.300(± 0.063)	21	0.72
	Global	0.606	0.503(± 0.063)	0.120(± 0.027)	188	0.45

^aThe results for the (stepwise) multilinear regression analyses are displayed here. They include coefficients, standard deviations (SD), the number of stations, and the fraction of the variance explained by the model (r^2) for each analysis. The term that is more influential to changes in Δ is given in bold (b_2 , ph; b_3 , CDM). When no coefficient is given, the term was considered to be insignificant in the regression.

value of its Southern Ocean counterparts. The Pacific Ocean stations, which are underestimated by the algorithm, have a median $a_{ph443}/Chla$ value of 0.042.

[34] In addition to $a_{ph443}/Chla$, phytoplankton community structure was examined using the model for cell size derived from *Ciotti et al.* [2002]. This model represents absorption spectra from mixed populations as a linear combination of picoplankton and microplankton absorption spectra. The effect of cell size was comparable to that of $a_{ph443}/Chla$ (results not shown). Small-size cells were associated with high values of $a_{ph443}/Chla$ and large cells with low values of $a_{ph443}/Chla$.

4.4. Possible Artifact: Normalization by $Chla$

[35] Although $a_{cdm443}/Chla$ and $a_{ph443}/Chla$ varied systematically with Δ (Figures 5 and 6), we considered the possibility that this might be an artifact of the normalization by $Chla$, since $Chla$ varies by as much as an order of magnitude at any fixed value of MBR. To test for this possibility, the station measurements of a_{cdm443} and a_{ph443} were randomly permuted and then normalized by the stations' original $Chla$. The systematic patterns associated with a_{cdm443} and a_{ph443} disappeared, indicating that the effects were not artifactual.

4.5. Covariation of the Two Effects

[36] The fact that Δ varies systematically with both $a_{cdm443}/Chla$ and $a_{ph443}/Chla$ suggests that a_{cdm443} and a_{ph443} systematically vary with each other. However, this proved to be true primarily only for the Atlantic coastal waters ($r^2 = 0.66$) (Table 4 and Figure 7). The relationship between a_{cdm443} and a_{ph443} sorted by water classes and color coded by ocean is shown in Figure 7. The absorption coefficients are plotted in the top row and the parameters, $a_{cdm443}/Chla$ and $a_{ph443}/Chla$, are plotted in the bottom row. Normalization by $Chla$ reduced the variability in a_{ph443} as noted by the narrower horizontal spread in the lower plots compared with those in the top row. Normal-

izing a_{cdm443} by $Chla$ had little effect on its variability. It is notable that $a_{cdm443} > a_{ph443}$ at nearly all of the Atlantic coastal stations, and at most stations in the other two ocean classes.

4.6. Relative Importance of CDM and Community Structure

[37] The covariation of a_{cdm443} and a_{ph443} was the motivation for using a stepwise regression of the form shown in equation (9). Table 5 lists the coefficients, standard deviations, the number of stations in the subset, and the fraction of the variance explained by the model (r^2) for each analysis. The coefficient shown in bold corresponds to the parameter that explains more of the variance, and hence, has the stronger influence.

[38] Overall, CDM had a stronger influence on algorithm uncertainty than the pigment effect. For the water class analysis, CDM had the stronger influence for the coastal and intermediate classes, while community structure had the stronger influence for the open ocean category. For analysis of the data sorted by both ocean and water class, the CDM effect was stronger in all categories except the Atlantic open ocean and coastal areas. In the case of the coastal Atlantic class, both CDM and the pigment effect were of equal importance. Their correlations with Δ (0.614 and 0.624, respectively) are not significantly different.

5. Discussion

5.1. Validation and Explanation of the Algorithm Uncertainty Through Inherent Optical Properties

[39] Using in situ radiometric measurements in NOMAD, we showed that the OC4v.6 algorithm incurred oceanic biases in its $Chla$ estimates. Possible artifacts associated with measurement techniques and data sources had previously been ruled out. We showed that similar biases existed when approximating the maximum band ratio with a ratio of total absorption coefficients. We accounted for the influence of particle size on the spectral slope of backscattering [Morel and Ahn, 1990, 1991; Stramski et al., 2004] using different models and found that the oceanic biases remained. Because the IOP measurements were produced independently from the radiometric measurements, the similarity in biases indicates that the oceans exhibit true differences in their inherent optical properties.

[40] When evaluating the effects of CDM and phytoplankton community structure separately, the parameters $a_{cdm443}/Chla$ and $a_{ph443}/Chla$ clearly exhibited systematic variation with algorithm biases. In regions where the algorithm overestimates $Chla$, both $a_{cdm443}/Chla$ and $a_{ph443}/Chla$ were relatively high. A result such as this is not unexpected since the algorithm is attributing spectral variability solely to chlorophyll a, whereas other substances (e.g., CDM) and pigment packaging are contributing to the variability in R_{rs} . What was unexpected were the systematic differences among the oceans with respect to these known effects.

[41] The effect of variability in the phytoplankton community structure was examined through the parameter $a_{ph443}/Chla$, the chlorophyll-specific absorption coefficient at 443 nm, and also with the use of a size parameter, S_f , from the model of *Ciotti et al.* [2002]. The algorithm under-

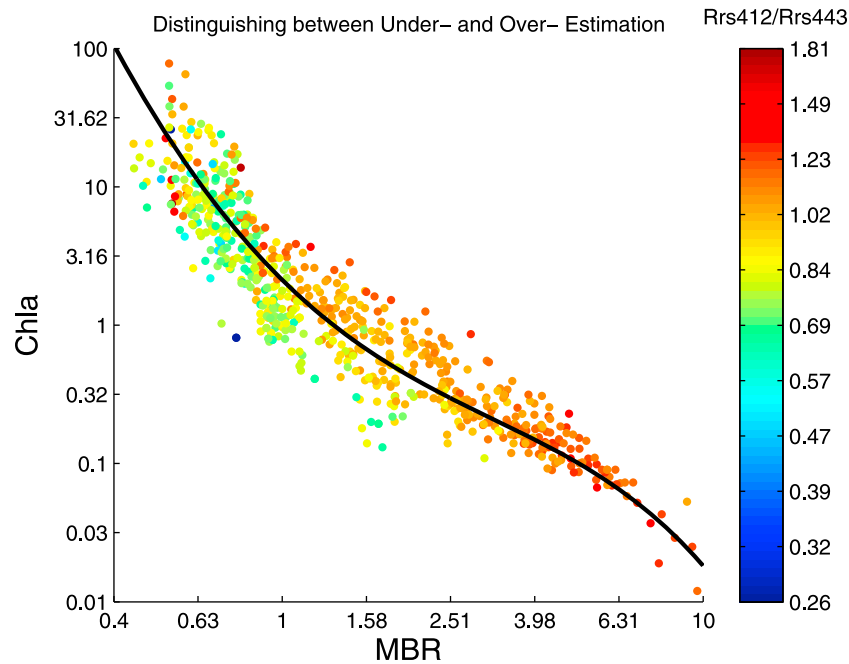


Figure 8. Distinguishing between under- and overestimation for the intermediate water class. R_{rs412}/R_{rs443} is color coded over the $Chla$ -MBR relationship. This ratio may be useful in distinguishing between under- and overestimations for the intermediate water class. Note that the axes and color scales are logarithmic.

estimated $Chla$ at Pacific stations characterized by low values of $a_{ph443}/Chla$ indicative of phytoplankton with large, highly packaged cells. By contrast, the algorithm overestimated $Chla$ at Atlantic stations characterized by relatively high values of $a_{ph443}/Chla$, associated with smaller, less packaged cells.

[42] The effect of CDM was examined through the parameter $a_{cdm443}/Chla$. In the context of algorithm uncertainty, $a_{cdm443}/Chla$ represents the extent to which CDM absorption is mistaken for chlorophyll absorption. The effect of CDM on algorithm uncertainty was consistent with expectation. When CDM was abundant, i.e., $a_{cdm443}/Chla$ was high, $Chla$ was overestimated, a situation that explains the Atlantic's positive bias. Relatively low levels of CDM compared with the Atlantic explain the Pacific's negative bias. Very few stations in the Southern Ocean had absorption measurements, but where these were available, they were consistent with results for the Pacific Ocean where $Chla$ was underestimated.

[43] By normalizing each absorption term by $Chla$, which is common for a_{ph443} but not for a_{cdm443} , the two parameters could be compared with the relative error, \hat{C}_i/C_i , which is also normalized by $Chla$. Both parameters considered together were used to explain variability in the algorithm uncertainty Δ , through a stepwise linear regression analysis. In general, it was found that the CDM effect explained more of the variance in Δ than community structure. This was true everywhere except the open ocean Atlantic, and in many locations, the effect of community structure was negligible (Table 5).

[44] Historically, empirical algorithms have been justified by assuming that optically active constituents, such as CDM, covary with $Chla$. To the extent that CDM does not

covary with $Chla$, its effect would increase the uncertainty. This is borne out by the correlations shown in Table 4, which show that the correlation between $\log_{10}a_{cdm443}$ and $\log_{10}Chla$ is systematically lower than that of $\log_{10}a_{ph443}$ and $\log_{10}Chla$. We speculate that this accounts for why the parameter, $a_{cdm443}/Chla$, is a better predictor of Δ than $a_{ph443}/Chla$ in most subsets.

[45] Another parameter that could explain the algorithm biases is $b_{bp}/Chla$. Loisel *et al.* [2010] presented $b_{bp}/Chla$ as a significant factor affecting algorithm estimates of $Chla$. The variability of this property is attributable to particle size distribution, refractive index, and the variation in shape of the particulate matter [Loisel *et al.*, 2010]. This parameter could explain the variability in the residuals after accounting for the effects of CDM and community structure. Unfortunately, we had insufficient backscattering data to include this in our analysis.

5.2. Applications to Ocean Color Algorithms

[46] While $a_{ph443}/Chla$ and $a_{cdm443}/Chla$ help explain the oceanic biases (equation (9)), they cannot be used directly to correct for the actual biases. Use of semianalytic algorithms that estimate the absorption coefficients could potentially resolve these issues. Based on Morel and Gentili [2009], the term R_{rs412}/R_{rs443} may also be considered for this purpose. Indeed, it appears possible to at least distinguish between under- and overestimations for the intermediate class using this ratio (Figure 8). The overestimated intermediate points are generally yellow and green whereas the underestimated intermediate points are orange and red. This would suggest that the inclusion of this band ratio in algorithms would improve $Chla$ estimates.

Table A1. Ocean-Specific OC4 Algorithms^a

Ocean	<i>N</i>	<i>r</i> ²	<i>a</i> ₀	<i>a</i> ₁	<i>a</i> ₂	<i>a</i> ₃	<i>a</i> ₄
Atlantic	1249	0.8869	0.2052	-3.4654	2.8954	2.4423	-3.9138
Pacific	595	0.8827	0.5109	-3.0871	1.1427	0.7416	-0.523
Southern	400	0.846	0.6728	-2.3832	-0.3546	2.2753	-2.2788

^aThe coefficients for the ocean-specific OC4 algorithms are presented for the Atlantic, Pacific, and Southern Oceans to demonstrate the ocean-specific biases in the global algorithm. The following format is used: $\log_{10}(Chla) = a_0 + a_1X + a_2X^2 + a_3X^3 + a_4X^4$, where *X* is MBR and *a*₀, *a*₁, *a*₂, *a*₃, and *a*₄ are the coefficients. In addition, the table includes the sample sizes, *n*, for each ocean-specific subset from NOMAD (*n* = 2365) and the fraction of the variance of the ocean-specific $\log_{10}(Chla)$ that is explained by the regression (*r*²).

5.3. Why Oceanic Differences in CDM and Phytoplankton Community Structure?

[47] Ultimately, optical differences in the world's oceans are related to oceanic differences in their ecological and biogeochemical processes. The relative abundance of CDM and its optical properties are dependent on its origin and mixing history [Boyd and Osburn, 2004; Stedmon *et al.*, 2011; Siegel *et al.*, 2002], including differences in the oceans' deep water chemistry [Swan *et al.*, 2009; Biscaye *et al.*, 1976; Kolla *et al.*, 1976; Berger *et al.*, 1976; Berger, 1972; Rickaby *et al.*, 2010; Jones *et al.*, 1995], riverine inputs, ocean-atmosphere interactions, photobleaching activity, and coastal phenomena [Cai, 2008; Cai *et al.*, 2006], and the biological composition (CDOM generated from grazing, and the degradation of bacteria and viruses) [Romera-Castillo *et al.*, 2010; Ortega-Retuerta *et al.*, 2009]. The characterization of the pigment packaging and accessory pigments is arguably governed by the environmental factors that shape the natural selection of phytoplankton communities, namely the intensity of light, the availability of various nutrients, grazing pressure, and the level of turbulence, and all of these attributes differ by ocean and water class [Longhurst, 2007].

[48] Although we have focused on ocean-specific algorithm biases, our results have broader implications than those about algorithm uncertainty. What is interesting here is that the world's oceans have systematic differences in their optical properties, and that these differences stem from the regional differences in biogeochemical and ecological processes. Such differences have been reported in the literature from regional studies [Mueller and Lange, 1989], and studies based on models and remotely sensed radiometry [Longhurst *et al.*, 1995; Siegel *et al.*, 2005]. Here, we contribute to the discussion with a global in situ data set. The original NOMAD data set, with 2,365 stations, was large enough to have sufficient representation of the different oceans (though less so for the Indian) for patterns to emerge. With the algorithm curve serving as a fixed reference, it was possible to observe systematic differences in the relationship between the spectral shape of reflectance and the chlorophyll concentration.

5.4. Caveat to the Oceanic Biases

[49] While the explanation for the source of the oceanic biases can be considered robust, the question of whether the NOMAD data represent their respective oceans remains.

The oceanic biases exist primarily in coastal and intermediate regions, both in the entire data set (*n* = 2365) and in the subset (*n* = 696) of stations with absorption measurements. However, the majority of stations in the subset are from regions less than 100 miles off the coast. The Pacific Ocean stations are mainly from the Southern California coast, the East China Sea, the Sea of Japan, and the coast of Northern Alaska. In the Southern Ocean, the stations are all from the Drake Passage and Bransfield Strait off the tip of the Western Antarctic Peninsula. In the Atlantic Ocean, 70% of the intermediate stations are from the Western Florida Shelf.

[50] In fact, an analysis of SeaWiFS data reveals locations where the 490 nm band was used to calculate *Chla*, which by our definition are intermediate waters. Some of the intermediate class regions not covered in NOMAD (*n* = 696) include the Malvinas current off the southeast coast of South America, the Benguela current off the southwest coast of Africa, and the northern section of the entire North Atlantic Ocean in which the spring bloom occurs annually. Consequently, it is possible that regions with an absence or lack of stations would have different results.

[51] Despite the caveat, the fact remains that the oceanic biases found in this subset (*n* = 696) also appear in the entire data set (*n* = 2365), which has a significantly larger spatial coverage. Hence, we recognize the significance of these oceanic differences in optical properties.

6. Conclusions

[52] Based on the analysis of NOMAD data at stations where both reflectance and absorption were measured, the world's oceans are, in fact, optically different, and these optical differences can be attributed to variations in the relative abundance of colored detrital matter (CDM), phytoplankton cell sizes, accessory pigments, and the extent to which pigments are packaged within the cells. We believe that regional differences in the water's optical properties are intrinsically related to differences in the ecological and biogeochemical processes of the regions. Considering that different regions in the analysis were characterized by different inherent optical properties, such work supports the use of ocean color radiometry to define ecological provinces.

[53] At the same time, we raise a concern for the limited spatial coverage of the NOMAD data upon which we based our results. Thus, we do not yet suggest the application of ocean-based algorithms. Unobserved regions may exhibit bio-optical properties different from those of our analysis. Such concerns emphasize the importance of consolidating regional data sets for facilitating a better understanding of global ecological provinces.

Appendix A: Ocean-Specific OC4 Algorithms

[54] The coefficients for ocean-specific OC4 algorithms are provided in Table A1, and the algorithms are illustrated with the global OC4v.6 algorithm in Figure A1. These algorithms are presented for the purpose of demonstrating the oceanic biases relative to the global algorithm. They should be used with caution. The in situ data are regionally limited within each ocean, and the coefficients would presumably change as new data are accumulated.

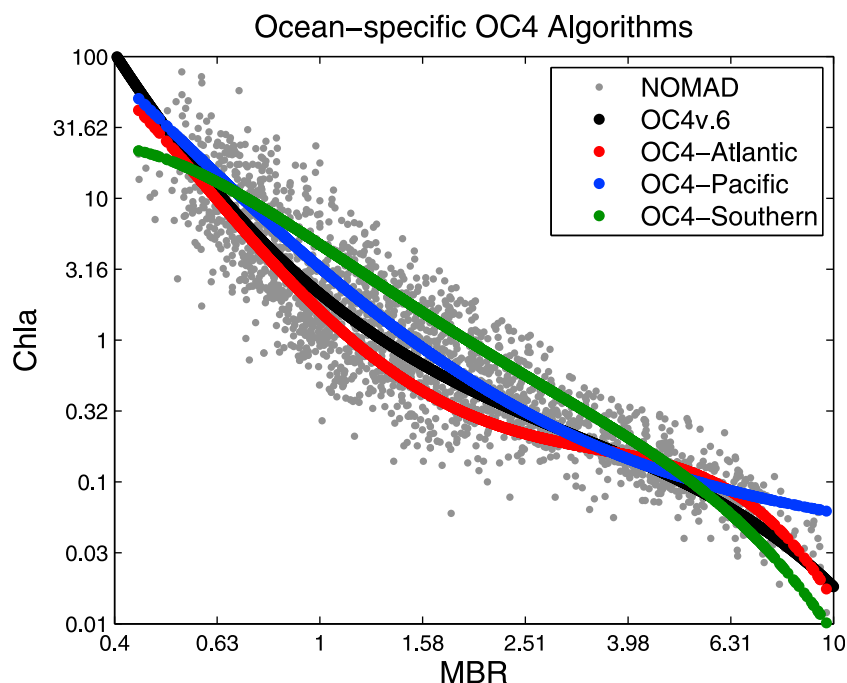


Figure A1. Ocean-specific OC4 algorithms. The ocean-specific OC4 algorithms (Atlantic, Pacific, and Southern) are shown with the global OC4v.6 algorithm on the plot of $Chla$ versus MBR (NOMAD, $n = 2365$). Note that the axes have logarithmic scales.

[55] **Acknowledgments.** This work was funded by the Research and Discover Fellowship Program cosponsored by NASA and the University of New Hampshire and a NASA grant to J. W. Campbell (NNX08AG80A). The authors would like to thank all of the Ocean Biology Processing Group members at NASA Goddard Space Flight Center for their guidance, as well as the contributors to the SeaBASS archive, making the comprehensive NOMAD data set available for analysis. Much gratitude also goes to the three anonymous reviewers of the manuscript, whose comments greatly strengthened the work and motivated a deeper investigation of the underlying questions.

References

- Ahn, Y. H., P. Shanmugam, J. E. Moon, and J. H. Ryu (2008), Satellite remote sensing of a low-salinity water plume in the East China Sea, *Ann. Geophys.*, 26(7), 2019–2035.
- Berger, W. (1972), Cretaceous and tertiary deep-sea sediments from Atlantic Ocean, *Am. Assoc. Pet. Geol. Bull.*, 56, 604.
- Berger, W. H., C. G. J. Adelseck, and L. Mayer (1976), Distribution of carbonate in surface sediments of the Pacific Ocean, *J. Geophys. Res.*, 81(15), 2617–2627.
- Biscaye, P. E., V. Kolla, and K. K. Turekian (1976), Distribution of calcium carbonate in surface sediments of the Atlantic Ocean, *J. Geophys. Res.*, 81(15), 2595–2603.
- Boyd, T., and C. Osburn (2004), Changes in CDOM fluorescence from allochthonous and autochthonous sources during tidal mixing and bacterial degradation in two coastal estuaries, *Mar. Chem.*, 89(1–4), 189–210.
- Bricaud, A., and D. Stramski (1990), Spectral absorption coefficients of living phytoplankton and nonalgal biogenous matter: A comparison between the Peru upwelling area and the Sargasso Sea, *Limnol. Oceanogr.*, 35(3), 562–582.
- Bricaud, A., A. Bedhomme, and A. Morel (1988), Optical properties of diverse phytoplanktonic species: Experimental results and theoretical interpretation, *J. Plankton Res.*, 10(5), 851–873.
- Cai, W. (2008), A comparative overview of weathering intensity and HCO_3^- flux in the world's major rivers with emphasis on the Changjiang, Huanghe, Zhujiang (Pearl) and Mississippi Rivers, *Cont. Shelf Res.*, 28(12), 1538–1549.
- Cai, W. J., M. H. Dai, and Y. C. Wang (2006), Air-sea exchange of carbon dioxide in ocean margins: A province-based synthesis, *Geophys. Res. Lett.*, 33, L12603, doi:10.1029/2006GL026219.
- Campbell, J. (1995), The lognormal distribution as a model for bio-optical variability in the sea, *J. Geophys. Res.*, 100(C7), 13,237–13,254.
- Ciotti, A., M. Lewis, and J. Cullen (2002), Assessment of the relationships between dominant cell size in natural phytoplankton communities and the spectral shape of the absorption coefficient, *Limnol. Oceanogr.*, 47(2), 404–417.
- Darecki, M., and D. Stramski (2004), An evaluation of MODIS And SeaWiFS bio-optical algorithms in the Baltic Sea, *Remote Sens. Environ.*, 89(3), 326–350, doi:10.1016/j.rse.2003.10.012.
- Dmitriev, E. V., G. Khomenko, M. Chami, A. A. Sokolov, T. Y. Churilova, and G. K. Korotaev (2009), Parameterization of light absorption by components of seawater in optically complex coastal waters of the Crimea Peninsula (Black Sea), *Appl. Opt.*, 48(7), 1249–1261.
- D'Ortenzio, F., S. Marullo, M. Ragni, M. D'Alcala, and R. Santoleri (2002), Validation of empirical SeaWiFS algorithms for chlorophyll-a retrieval in the Mediterranean Sea: A case study for oligotrophic seas, *Remote Sens. Environ.*, 82(1), 79–94.
- Fenton, N., J. Priddle, and P. Tett (1994), Regional variations in bio-optical properties of the surface waters in the Southern Ocean, *Antarct. Sci.*, 6(4), 443–448.
- Garcia, C., V. Garcia, and C. McClain (2005), Evaluation of SeaWiFS chlorophyll algorithms in the southwestern Atlantic and Southern Oceans, *Remote Sens. Environ.*, 95(1), 125–137, doi:10.1016/j.rse.2004.12.006.
- Gohin, F., J. Druon, and L. Lampert (2002), A five channel chlorophyll concentration algorithm applied to SeaWiFS data processed by SeaDAS in coastal waters, *Int. J. Remote Sens.*, 23(8), 1639–1661, doi:10.1080/01431160110071879.
- Gordon, H., O. Brown, R. H. Evans, J. W. Brown, R. C. Smith, K. S. Baker, and D. K. Clark (1988), A semianalytic radiance model of ocean color, *J. Geophys. Res.*, 93(D9), 10,909–10,924.
- International Ocean Colour Coordinating Group (2009), Partition of the ocean into ecological provinces: Role of ocean-colour radiometry, *IOCCG Rep. 9*, edited by M. Dowell and T. Platt, Dartmouth, N. S., Canada.
- Jones, E. P., B. Rudels, and L. Anderson (1995), Deep waters of the Arctic Ocean origins and circulation, *Deep Sea Res. Part I*, 42(5), 737–760.
- Kahru, M., and B. Mitchell (1999), Empirical chlorophyll algorithm and preliminary SeaWiFS validation for the California Current, *Int. J. Remote Sens.*, 20(17), 3423–3429.
- Kirk, J. (1994), *Light and Photosynthesis in Aquatic Ecosystems*, 2nd ed., 509 pp., Cambridge Univ. Press, Cambridge, U. K.
- Kolla, V., A. W. Be, and P. E. Biscaye (1976), Calcium carbonate distribution in the surface sediments of the Indian Ocean, *J. Geophys. Res.*, 81(15), 2605–2616.

- Lee, Z., K. Carder, and R. Arnone (2002), Deriving inherent optical properties from water color: A multiband quasi-analytical algorithm for optically deep waters, *Appl. Opt.*, **41**(27), 5755–5772.
- Lee, Z., R. Arnone, C. M. Hu, P. J. Werdell, and B. Lubac (2010), Uncertainties of optical parameters and their propagations in an analytical ocean color inversion algorithm, *Appl. Opt.*, **49**(3), 369–381.
- Loisel, H., B. Lubac, D. Dessailly, L. Dufor-Gaurier, and V. Vantrepotte (2010), Effect of inherent optical properties variability on the chlorophyll retrieval from ocean color remote sensing: An in situ approach, *Opt. Express*, **18**(20), 20,949–20,959.
- Longhurst, A. (2007), *Ecological Geography of the Sea*, 2nd ed., Academic, Amsterdam.
- Longhurst, A., S. Sathyendranath, T. Platt, and C. Caverhill (1995), An estimate of global primary production in the ocean from satellite radiometer, *J. Plankton Res.*, **17**(6), 1245–1271.
- Lutz, V. A., A. Subramaniam, R. M. Negri, R. I. Silva, and J. I. Carreto (2006), Annual variations in bio-optical properties at the 'Estacion Permanente de Estudios Ambientales (Epea)' coastal station, Argentina, *Cont. Shelf Res.*, **26**(10), 1093–1112, doi:10.1016/J.Csr.2006.02.012.
- Maritorena, S., D. Siegel, and A. Peterson (2002), Optimization of a semi-analytical ocean color model for global-scale applications, *Appl. Opt.*, **41**(15), 2705–2714.
- Maske, H., and H. Haardt (1987), Quantitative in vivo absorption spectra of phytoplankton: Detrital absorption and comparison with fluorescence excitation spectra, *Limnol. Oceanogr.*, **32**(3), 620–633.
- Mitchell, B., and O. Holm-Hansen (1991), Observations and modeling of the Antarctic phytoplankton crop in relation to mixing depth, *Deep Sea Res. Part A*, **38**(8–9), 981–1007.
- Mitchell, B., and D. Kiefer (1988a), Chlorophyll-alpha specific absorption and fluorescence excitation-spectra for light-limited phytoplankton, *Deep Sea Res. Part A*, **35**(5), 639–663.
- Mitchell, B., and D. Kiefer (1988b), Variability in pigment specific particulate fluorescence and absorption spectra in the northeastern Pacific Ocean, *Deep Sea Res. Part A*, **35**(5), 665–689.
- Moore, T., J. Campbell, and M. Dowell (2009), A class-based approach for characterizing the uncertainty of the MODIS chlorophyll product, *Remote Sens. Environ.*, **113**, 2424–2430.
- Morel, A. (1974), Optical properties of pure water and pure seawater, in *Optical Aspects of Oceanography*, edited by N. Jerlov and E. Nielsen, pp. 1–24, Academic, London.
- Morel, A. (1980), In-water and remote measurements of ocean color, *Boundary Layer Meteorol.*, **18**(2), 177–201.
- Morel, A., and Y.-H. Ahn (1990), Optical efficiency factors of free-living marine bacteria: Influence of bacterioplankton upon the optical properties and particulate organic carbon in oceanic waters, *J. Mar. Res.*, **48**, 145–175.
- Morel, A., and Y. Ahn (1991), Optics of heterotrophic nanoflagellates and ciliates: A tentative assessment of their scattering role in oceanic waters compared to those of bacterial and algal cells, *J. Mar. Res.*, **49**(1), 177–202.
- Morel, A., and B. Gentili (2009), A simple band ratio technique to quantify the colored dissolved and detrital organic material from ocean color remotely sensed data, *Remote Sens. Environ.*, **113**, 998–1011.
- Morel, A., and S. Maritorena (2001), Bio-optical properties of oceanic waters: A reappraisal, *J. Geophys. Res.*, **106**(C4), 7163–7180.
- Morel, A., H. Claustre, D. Antoine, and B. Gentili (2007), Natural variability of bio-optical properties in case 1 waters: Attenuation and reflectance within the visible and near-UV spectral domains, as observed in South Pacific and Mediterranean Waters, *Biogeosciences*, **4**(5), 913–925.
- Morrow, J., W. Chamberlin, and D. Kiefer (1989), A two-component description of spectral absorption by marine particles, *Limnol. Oceanogr.*, **34**(8), 1500–1509.
- Mueller, J. L., and R. E. Lange (1989), Bio-optical provinces of the northeast Pacific Ocean: A provisional analysis, *Limnol. Oceanogr.*, **34**(8), 1572–1586.
- O'Reilly, J., et al. (2002), Ocean color chlorophyll a algorithms for SeaWiFS, OC2, and OC4: Version 4, in *Volume 11, SeaWiFS Postlaunch Calibration and Validation Analyses, Part 3*, edited by J. E. O'Reilly et al., NASA/TM-2000-206892, pp. 9–23, NASA Goddard Space Flight Cent., Greenbelt, Md.
- Ortega-Retuerta, E., T. Frazer, C. Duarte, S. Ruiz-Halpern, A. Tovar-Sanchez, J. Arrieta, and I. Reche (2009), Biogeneration of chromophoric dissolved organic matter by bacteria and krill in the Southern Ocean, *Limnol. Oceanogr.*, **54**(6), 1941–1950.
- Pan, X., A. Mannino, M. E. Russ, and S. B. Hooker (2008), Remote sensing of the absorption coefficients and chlorophyll a concentration in the United States southern Middle Atlantic Bight from SeaWiFS and MODIS-Aqua, *J. Geophys. Res.*, **113**, C11022, doi:10.1029/2008JC004852.
- Rickaby, R. E. M., H. Elderfield, N. Roberts, C. D. Hillenbrand, and A. Mackensen (2010), Evidence for elevated alkalinity in the glacial Southern Ocean, *Paleoceanography*, **25**, PA1209, doi:10.1029/2009PA001762.
- Romera-Castillo, C., H. Sarmiento, X. A. Alvarez-Salgado, J. M. Gasol, and C. Marrase (2010), Production of chromophoric dissolved organic matter by marine phytoplankton, *Limnol. Oceanogr.*, **55**(1), 446–454.
- Siegel, D., S. Maritorena, N. Nelson, D. Hansell, and M. Lorenzi-Kayser (2002), Global distribution and dynamics of colored dissolved and detrital organic materials, *J. Geophys. Res.*, **107**(C12), 3228, doi:10.1029/2001JC000965.
- Siegel, D., S. Maritorena, N. Nelson, and M. Behrenfeld (2005), Independence and interdependencies among global ocean color properties: Reassessing the bio-optical assumption, *J. Geophys. Res.*, **110**, C07011, doi:10.1029/2004JC002527.
- Stedmon, C., R. M. W. Amon, A. J. Rinehart, and S. A. Walker (2011), The supply and characteristics of colored dissolved organic matter (CDOM) in the Arctic Ocean: Pan-Arctic trends and differences, *Mar. Chem.*, **124**, 108–118.
- Stramski, D., E. Boss, D. Bogucki, and K. Voss (2004), The role of seawater constituents in light backscattering in the ocean, *Prog. Oceanogr.*, **61**(1), 27–56, doi:10.1016/J.Pocean.2004.07.001.
- Swan, C., D. Siegel, N. Nelson, C. Carlson, and E. Nasir (2009), Biogeochemical and hydrographic controls on chromophoric dissolved organic matter distribution in the Pacific Ocean, *Deep Sea Res. Part I*, **56**(12), 2175–2192.
- Werdell, P. (2005), *An evaluation of inherent optical property data for inclusion in the NASA Bio-optical Marine Algorithm Data Set*, NASA Ocean Biology Processing Group paper, NASA Goddard Space Flight Cent., Greenbelt, Md. [Available at http://seabass.gsfc.nasa.gov/seabass/data/werdell_nomad_iop_qc.pdf.]
- Werdell, P., and S. Bailey (2005), An improved in-situ bio-optical data set for ocean color algorithm development and satellite data product validation, *Remote Sens. Environ.*, **98**(1), 122–140, doi:10.1016/J.Rse.2005.07.001.
- Werdell, P. J., S. W. Bailey, B. A. Franz, L. W. Harding Jr., G. C. Feldman, and C. R. McClain (2009), Regional and seasonal variability of chlorophyll-a in Chesapeake Bay as observed by SeaWiFS and MODIS-Aqua, *Remote Sens. Environ.*, **113**(6), 1319–1330, doi:10.1016/J.Rse.2009.02.012.
- Zaneveld, J. (1995), A theoretical derivation of the dependence of the remotely-sensed reflectance of the ocean on the inherent optical-properties, *J. Geophys. Res.*, **100**(C7), 13,135–13,142.

J. W. Campbell, T. S. Moore, and M. Szeto, Ocean Process Analysis Laboratory, Institute for the Study of Earth, Oceans, and Space, University of New Hampshire, 8 College Rd., Morse Hall, Rm. 142, Durham, NH 03824, USA. (janet.campbell@unh.edu; timothy.moore@unh.edu; mimi.szeto@unh.edu)

P. J. Werdell, Ocean Biology Processing Group, NASA Goddard Space Flight Center, Mail Code 614.8, Greenbelt, MD 20771, USA. (jeremy.werdell@nasa.gov)